



# Fracture Dynamics of Sprayed and Laser-Glazed Titania by an Inverse Processing of Elastic Waves

*M. Takemoto, T. Nanbu, and Y. Hayashi*

A new elastic wave (EW) or acoustic emission (AE) monitoring and signal processing system has been developed and used to elucidate the fracture behavior of sprayed and laser-glazed ceramic coatings. The system measures the minute surface displacements excited by the propagation of elastic waves. It enables elucidation of the fracture dynamics (fracture mode and kinetics) of stressed coatings. The surface displacement at the sensor position was computed by the convolution integral of an assumed source wave with the dynamic Green's function until signals resembled the measured wave. This new signal processing method was used to determine the fracture strength and dynamics of microcracks in sprayed and laser-glazed titania subjected to four-point bending. It was found that mode II shear cracking along the interface between the coating and substrate occurred prior to mode I cleavage cracking. The fracture strength of laser-glazed titania was higher than that of as-sprayed titania in most cases; however, this depended on the coating structure. This article introduces the principle of source inversion processing of elastic waves, the monitoring system, laser glazing of sprayed titania, and experimental work on the fracture behavior of titania coatings.

## 1. Introduction

COATINGS deposited by thermal spraying usually contain a number of pores, unmelted particles, and cracks. Pores in the coating could be useful for thermal barrier coatings, but do not isolate the substrate from aggressive environments.<sup>[1]</sup> Laser glazing of sprayed oxide ceramics has been attempted<sup>[2-6]</sup> to eliminate the pores and paths throughout the coating. However, laser glazing of sprayed ceramics is difficult because of the high susceptibility to cracking and exfoliation.<sup>[7]</sup> Low fracture toughness, inferior bonding strength to the substrate, and localized thermal concentration due to the low thermal conductivity of ceramics make the glazing procedure difficult. One purpose of this article is to find an optimum laser irradiation condition to produce dense ceramic coatings.

On the other hand, fracture behavior in ceramic coatings under thermal or mechanical loading is complex and includes various cracks and delamination along the interface. Acoustic emission (AE) has been used widely to monitor the initiation and propagation of fracture in coatings. However, most AE methods analyze the detected waves, which are distorted by the unknown transfer function of the system (i.e., the physical processes that distort the AE wave within the media and monitoring system) and have difficulty characterizing the complex fracture modes

in the coating. It is not possible to obtain information on the fracture dynamics by analysis of the detected waves. It is also difficult to extract the important signals from noise when a conventional monitoring system is used. Special monitoring and signal processing are therefore necessary to obtain useful information on fracture dynamics. The authors developed a novel elastic wave (EW) monitoring system that measures surface displacements of the order of 0.02 Å and are successful in estimating the source wave of microfractures by an inversion processing method.<sup>[8,9]</sup> This signal processing, namely source inversion processing, is used to estimate the fracture mode and to determine the fracture strength of the coatings.

Another purpose of this article is to examine the fracture strength and crack dynamics of sprayed and laser-glazed titania coatings using the new signal processing system.

## 2. Elastic Wave Monitoring and Source Inversion Processing

Source inversion processing is a signal processing technique used to obtain source waves from detected waves that are distorted. The source wave of the fracture process (termed a "dipole problem" in the field of EW) contains direct information on the fracture dynamics such as the fracture mode, fracture kinetics, and generated crack volume. Source waves could be obtained by the deconvolution integral of detected waves from the overall transfer function if the system is linear. However, it is usually very difficult to determine the overall transfer function of the media and monitoring system, and this is absolutely necessary in the deconvolution process. On the other hand, source waves can be obtained when the minute surface displacement excited by propagation of the EW is measured.

**Keywords:** acoustic emission, cracking mode, fracture dynamics, Green's function, laser glazed ceramic, titania coatings

**M. Takemoto**, Prof. Faculty of Science and Engineering, Aoyama Gakuin University; **T. Nanbu**, Researcher, NTN Corporation; and **Y. Hayashi**, Fellow of the Japan Society for the Promotion of Science for Japanese Junior Scientist, Tokyo, Japan.

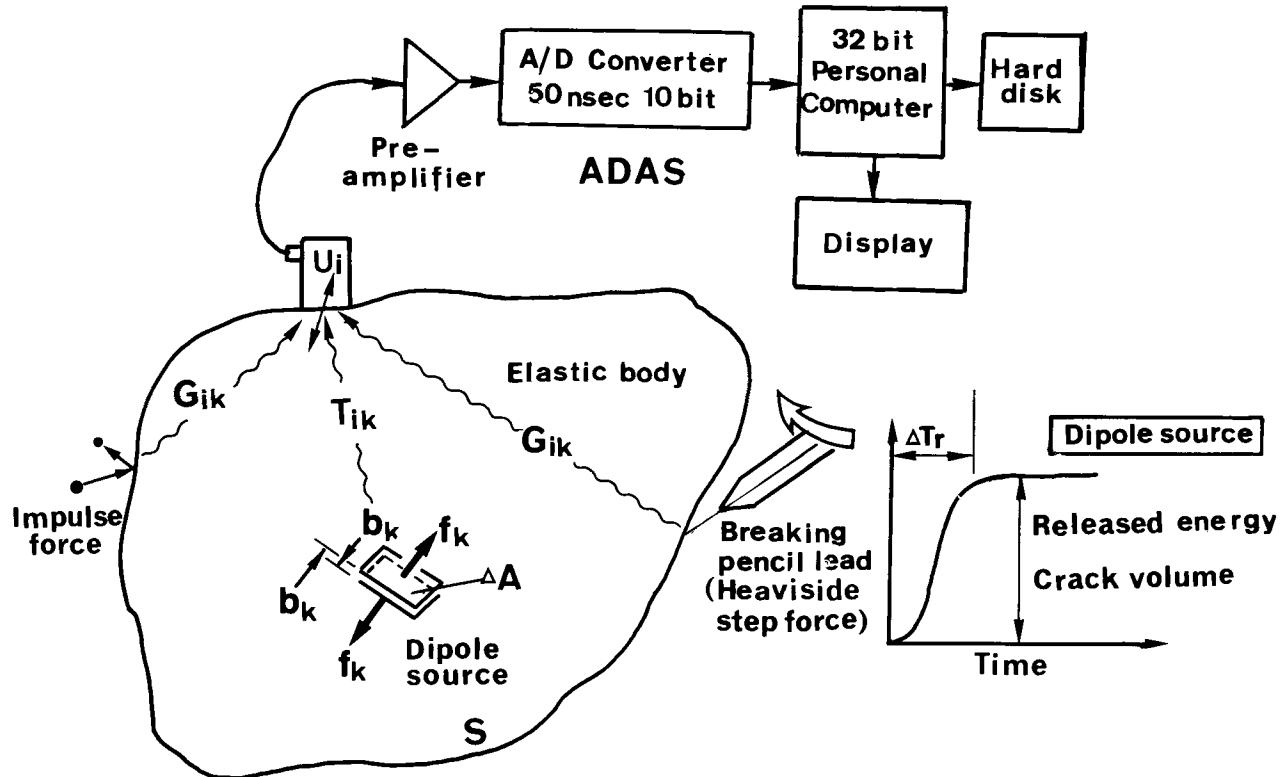


Fig. 1 Schematic of elastic wave source inversion processing. See text for explanation of symbols.

Figure 1 shows a schematic illustration of EW propagation and the monitoring system. The system is composed of a displacement-sensitive sensor (Dunegan S9208), a low noise, wide band preamplifier (NF Circuit Block Co. 9913), a fast analog/digital converter (Autonix S121), a 32-bit personal computer, and a hard disk. The frequency resolution of this system is 10 MHz, and it measures the minute displacement normal to the outer boundary,  $S$ , of an elastic body, and thus, the transfer function of the monitoring system may be ignored.

The principle of source inversion processing is briefly described. The displacement  $U_i(x, t)$  in the  $X_i$  direction on the elastic body at point  $x$  and time  $t$  produced by propagation of elastic waves is given by Eq 1 and 2 if the media is an isotropic elastic body:<sup>[10]</sup>

$$U_i(x, t) = \int_{-\infty}^{\infty} dt' \int^S G_{ik}(x; x', t-t') f_k(x', t') dS \quad [1]$$

$$U_i(x, t) = \int_{-\infty}^{\infty} dt' \int^S T_{ik}(x; x', t-t') b_k(x', t') dS \quad [2]$$

Equation 1 is valid for monopole sources such as an impulse force or a step force input. Equation 2 is valid for a dipole source such as a crack generated under the balanced force  $f_k$ . The term  $b_k$  in Eq 2 refers to crack-tip opening displacement (CTOD);  $G_{ik}(x, t; x', t')$ , and  $T_{ik}(x, t; x', t')$  are the Green's function of the first and second kind.  $T_{ik}$  is given by Eq 3:

$$T_{ik} = \lambda G_{ij, k} n_k + \mu G_{ik, j} n_j + \mu G_{ij, k} n_j \quad [3]$$

where  $\lambda$  and  $\mu$  are Lame's constants, and  $n_i$  is the unit vector normal to crack surface  $\Delta A$ .  $G_{ij, k}$  refers to the spatial deviative of  $G_{ij}$  in the  $x_k$  direction. When the source volume ( $\Delta A b_k$ ) is infinitesimal compared to the outer boundary, then Eq 1 and 2 are rewritten as the convolution integral in time (denoted by the symbol  $*$ ) as follows:

$$U_i(x, t) = G_{ik}(x, t; x', t') * f_k \Delta A(x', t') \quad [4]$$

$$U_i(x, t) = T_{ik}(x, t; x', t') * b_k \Delta A(x', t') \quad [5]$$

When a crack generates within  $\Delta T_r$  (where  $r$  refers to rise time) and then stops propagating, the source wave could be given by the step function of crack volume or the released energy, as shown in the inset in Fig. 1.

Because the analytical solution of Green's function has been determined by Johnson,<sup>[11]</sup> the source wave  $b_k \Delta A(x', t')$  can be obtained from the theoretical Green's function by the deconvolution integral of the displacement:

$$\Delta A b_k(x, t') = U_i(x, t) * [T_{ik}(x, t; x', t')]^{-1} \quad [6]$$

where  $*[ ]^{-1}$  denotes the deconvolution integral of the Green's function in the square brackets.

The EW theory strongly indicates that it is important to measure the surface displacement  $U_i(x, t)$ . The source wave can be obtained from the displacement when only the acoustic properties

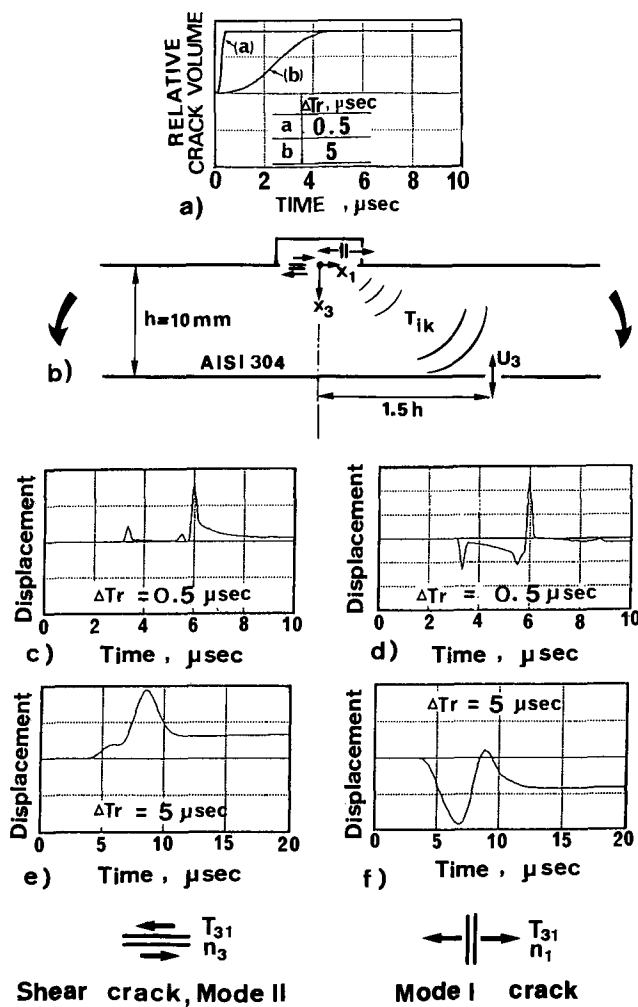


**Fig. 2** Simulated surface displacement at 1.5 h off-epicenter to mode I (d and f) and mode II (c and e) cracking. (a) Rise time response for cracks with different times. The experimental arrangement is shown in (b).

and the coordinates of the source point are given. Computer signal processing technology is used for convolution and deconvolution integrals in time and frequency domain. The data acquisition and analyzing system (ADAS) of the system can perform this signal processing.

Source inversion processing to characterize the fracture dynamics of sprayed coatings is more precisely shown in Fig. 2. Consider cracking in the coating deposited on a steel substrate of thickness  $h$  during four-point bending. Possible fractures are mode I vertical cracks in the coating and mode II shear cracking along the boundary between the substrate and coating. The displacement by mode II cracking at the epicenter is essentially zero, and therefore, the displacement sensitive sensor (S9208) was mounted at 1.5 h off-epicenter.

Waves in the lower part of Fig. 2 are the simulated displacements for mode II and mode I cracking in the coating. The source wave is approximated by the sinusoidal ramp function of Eq 7. Source waves with different rise times determined from Eq 7 are shown in Fig. 2(a):

$$\begin{aligned}\partial V(t)/\partial t &= V_0 \cdot \sin^4(\pi t/\Delta T_r) \quad \text{for } 0 < t < \Delta T_r, \\ &= V_0 \quad \text{for } \Delta T_r < t\end{aligned}\quad [7]$$

The phases of the longitudinal wave (P-wave) from mode I cracking and mode II are different (plus for mode I and minus for mode II), and the wave loses the high-frequency component with an increase in rise time, i.e., slow evolution of cracking.

In the case of such a sensor layout, the source wave is likely to diverge when a direct deconvolution integral of Eq 6 is used, because the displacement from the first P-wave is smaller than that by the following waves (shear, S, or SP waves). A forward (simulation) approach was used in this experiment to avoid instability of the source wave. The displacement at the sensor position was computed to an assumed source wave until the simulated displacement resembled the measured displacement.

If the amplitude of the displacement is measured, then the crack volume can be directly determined. However, crack volume was not taken into consideration for this experiment because of wave attenuation and reflection at the coating/substrate interface.

Whether the monitoring system measures displacement was examined using Eq 4; i.e., to measure the displacement produced by breaking a sharp pencil lead. The source wave of such a pencil test is a Heaviside step function with a released force of 3.5 N and a rise time of 0.9 μs.<sup>[12]</sup> Displacement was calculated from the convolution integral of the source wave (Eq 7 where the crack volume  $V$  was replaced by force) with the Heaviside Green's function  $G_{ik}^H(x, t; x', t')$ . Figure 3 compares the computed (Fig. 3b) and monitored (Fig. 3c) waves at the 1.5 h off-epicenter. The displacements caused by the first P- and following SP-waves were found to be correctly monitored by the experimental system.

### 3. Specimens and Experimental

Austenitic AISI 304 stainless steel with a sprayed and laser-glazed titania coating was submitted to four-point bending, as shown in Fig. 4. The crosshead speed was kept at 0.14 mm/min. Acoustic emission monitoring by the conventional system (a velocity-sensitive PZT sensor R15 and a signal processor PAC 3000) was also conducted. The outer fiber strain was measured with a strain gage mounted near the coating. The measured strains and the stresses calculated by elastic bending theory were used as parameters to measure the mechanical properties of the coating.

Titania powder (Metco 102) was sprayed by acetylene-oxygen gas flame spraying (Metco 5P gun) onto the central surface of the alumina grit-blasted AISI type 304 steel. The thickness of the coating was controlled to about 300 and 80 μm for as-sprayed and laser-glazed specimens, respectively. Glazing was performed by the scanning beam method with a carbon dioxide laser, as shown in Fig. 5.

In spite of extensive work on the laser glazing of thick titania coatings (300 to 500 μm) from 1986 to 1989, severe cracking in the remelted layer limited the thickness of coating that could be applied successfully (Fig. 6). However, experiments in 1989 determined that laser glazing of sprayed titania was possible under

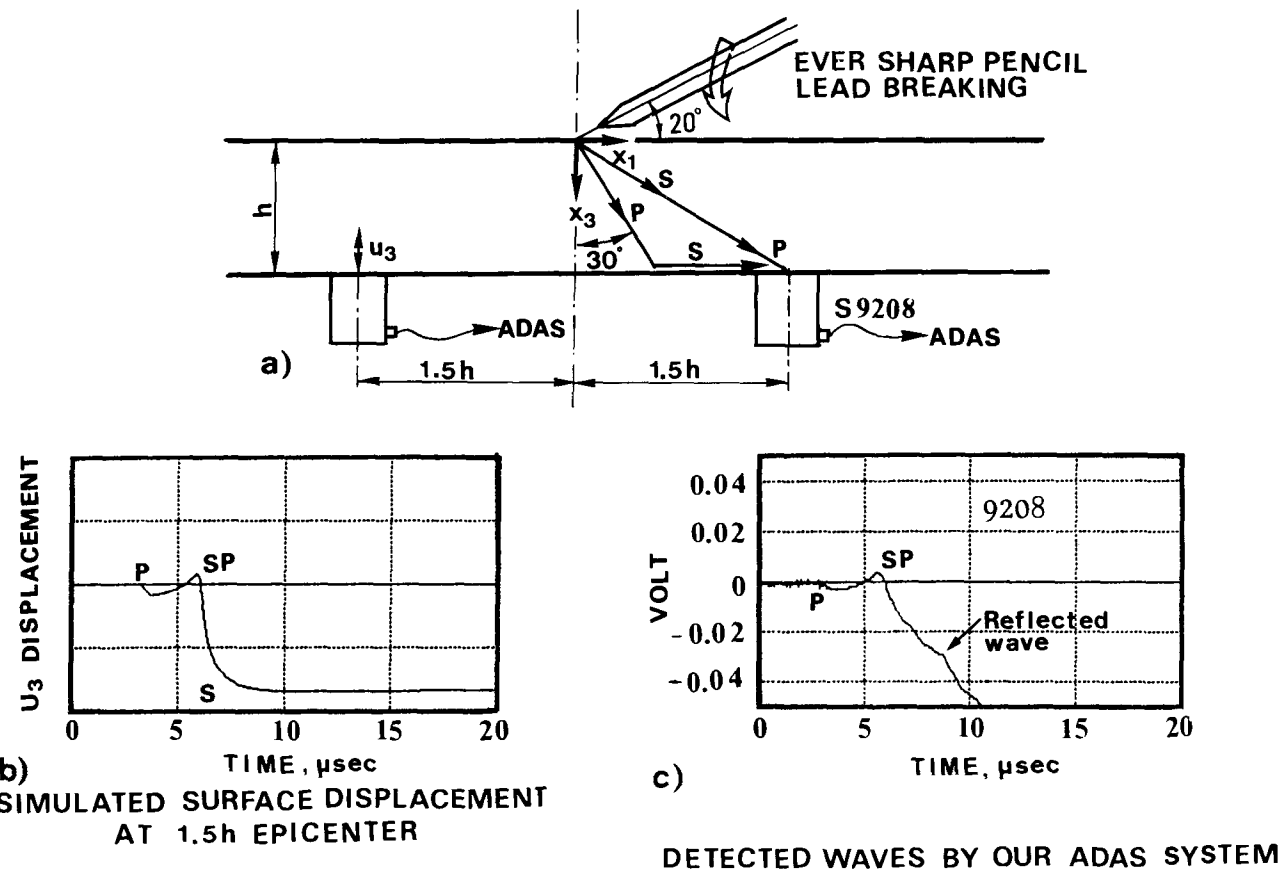


Fig. 3 Comparison of simulated displacement and detected waves by the ADAS for breaking sharp pencil lead.

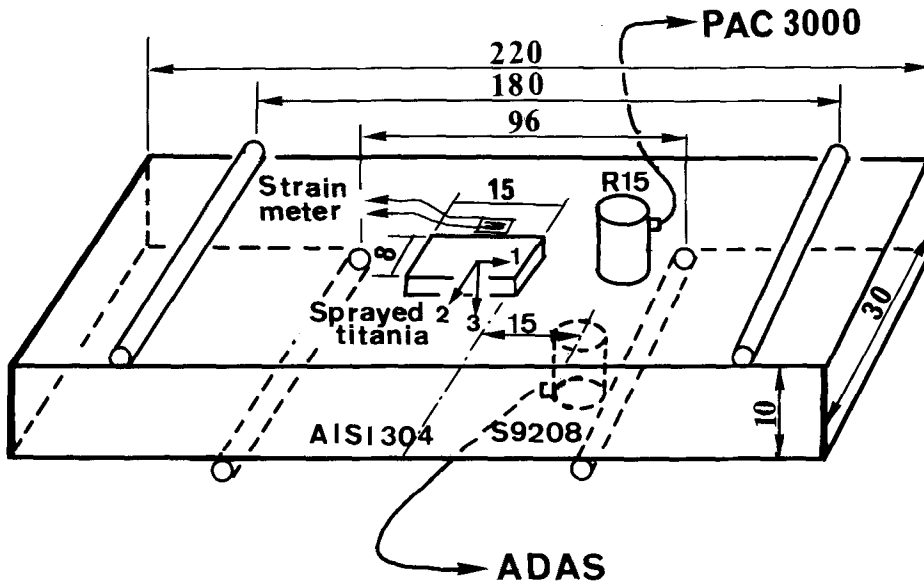
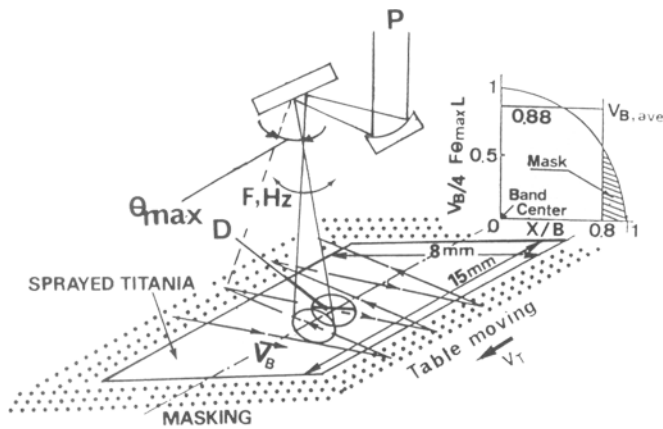


Fig. 4 Configuration of specimen and sensors for four-point bending. All dimensions are in millimeters.

very limited laser irradiation conditions (Fig. 7) when thin 80- $\mu\text{m}$  titania was fully fused to the chromium-bearing substrate steel. Chromia contributes to improved adhesion of the fused titania. However, the characteristics of the glazed layer such as the spacing and slant angle of the lamellar structure could not be

optionally controlled because the structure was produced during extremely rapid solidification. The mechanical characteristics of glazed coatings also seemed to depend on the structure, and therefore, these structures were examined by EW methods and compared to as-sprayed coatings.



$$V_B = 4\theta L = 4\pi F \theta_{\max} L \cdot \cos(2\pi F \theta)$$

$$V_B \text{ ave} = 0.88 \times 4\pi F \theta_{\max} L$$

$$\text{Dwell time; } t_d = D / \sqrt{V_T^2 + V_B^2}$$

$$\text{Power density; } P_d = P / \pi D^2 / 4$$

$$\text{Specific energy } E_s = P_d \times t_d$$

$$\text{Overlap number; } N = 2DF / V_T$$

Fig. 5 Scanning beam method for laser glazing of sprayed titania. Process parameters are given.

#### 4. Fracture Strength and Dynamics of As-Sprayed Titania

Two specimens (I and II) were submitted to the bend test. Figure 8 shows the ADAS output with respect to the stress-strain curve of specimen I. The first EW was detected at 93.7 MPa and correlated to mode II cracking, because the detected wave resembles the computed model (Fig. 2e). The wave detected at 94.2 MPa was produced under mode I cracking. The test was interrupted just after these two waves, and the specimen was submitted to metallographic examination. As shown in Fig. 9, vertical (mode I) and shear (exfoliation) cracks were observed in the central region of the coating.

Figure 10 shows the timing of the elastic waves of specimen II, as monitored by the ADAS and the PAC 3000. The numbers (1-5) near the arrows on the stress-time curve in the upper figure correspond to the number of elastic waves detected. A rapid increase in AE hits by the conventional monitoring system (lower figure) agrees well with the timing of the first EW by the ADAS. The conventional monitoring system could be used to monitor the beginning of fracture in the coating; however, it was not informative concerning fracture dynamics.

ADAS indicated that the first fracture at a stress of 116.5 MPa was caused by mode II cracking followed by mode I verti-

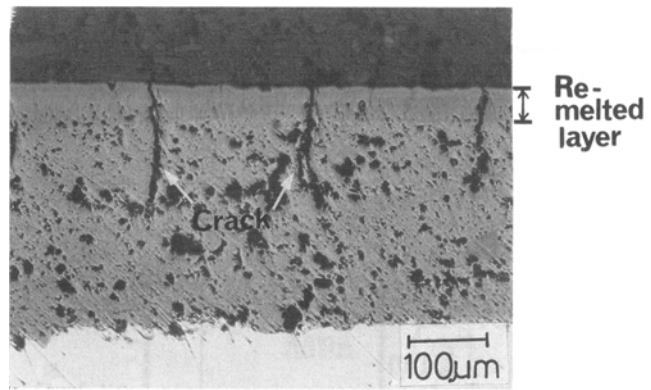


Fig. 6 Transverse SEM of laser-superficially glazed titania coating.

MIRROR FREQUENCY;  $F = 4.5 \text{ Hz}$

TABLE VELOCITY;  $V_T = 0.1 \text{ m/s}$

DEFOCUS DISTANCE = +4.5 mm

LASER POWER = 700–800 Watt

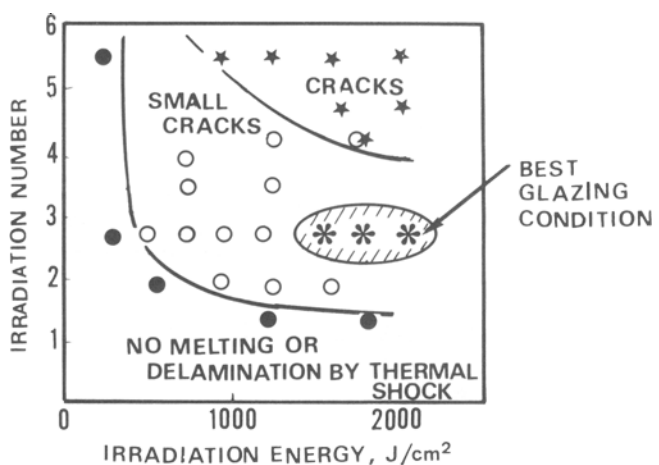


Fig. 7 Irradiation conditions for laser glazing of sprayed titania.

cal cracks in the as-sprayed titania. Generation of significant elastic waves suggests that cracking in the porous coating is not critical or that microcracks follow a repeated sequence of initiation and arrest.

#### 5. Fracture Strength and Dynamics of Laser-Glazed Titania

Four specimens with different lamellar structures were submitted to the bend test. Figure 11 shows the AE behavior in stress and strain versus time diagram for specimen III. There was an increase of AE hits around 20 min; however, the ADAS did not detect any signals around this time. The first EW was detected by the ADAS at 192.5 MPa and 0.117% strain. As shown in Fig. 12,

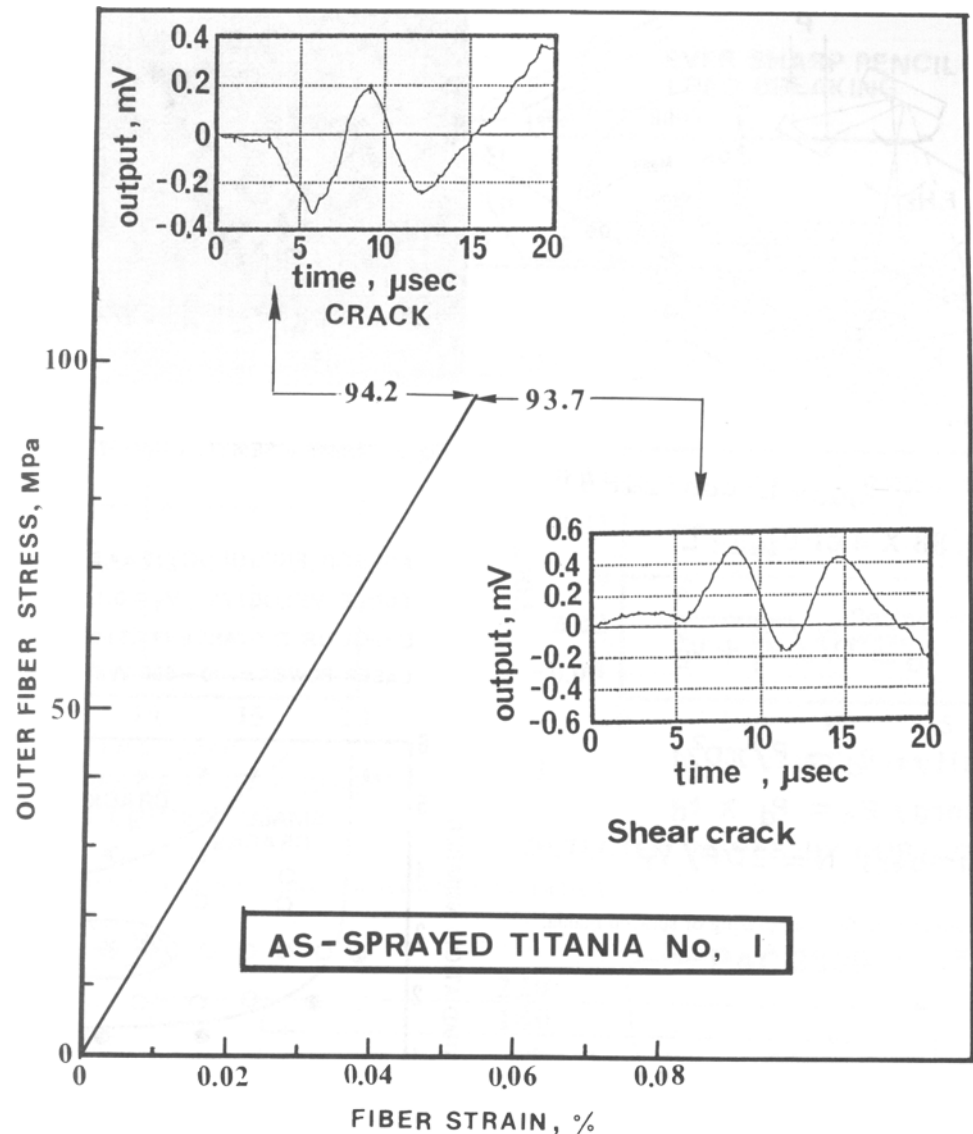


Fig. 8 Timing of elastic waves by the ADAS in the stress-strain diagram of as-sprayed titania (specimen I).

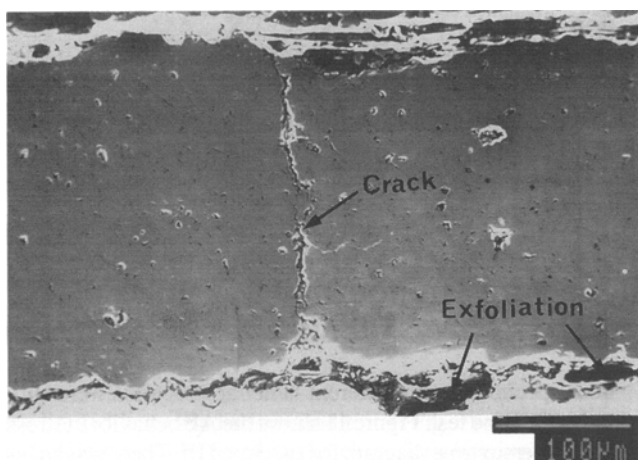
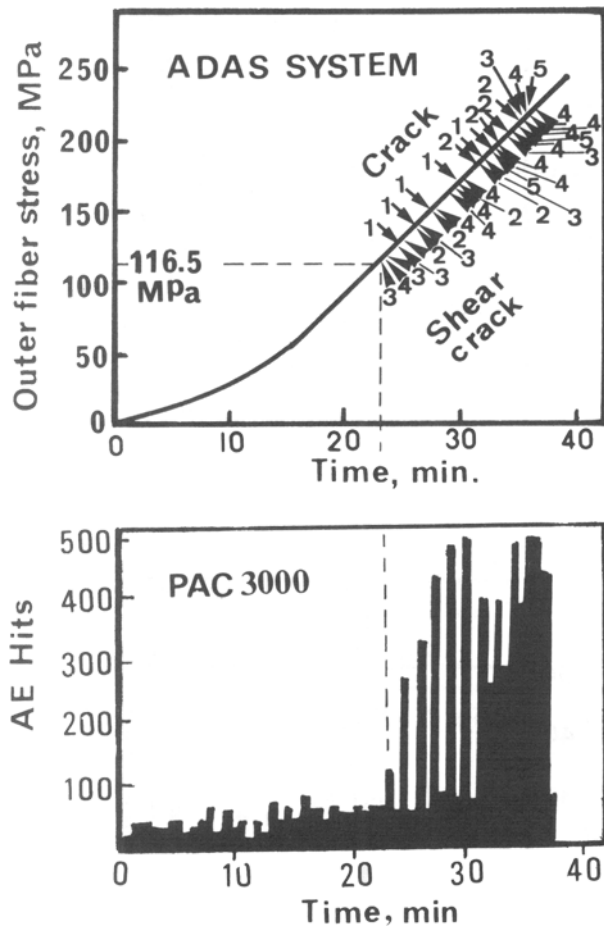


Fig. 9 Transverse SEM of specimen shown in Fig. 8 immediately after two elastic waves.

this wave possesses a positive phase of a P-wave and resembles the displacement computed to the mode II shear cracking with a rise time of 1  $\mu$ s. The slight difference between waves A and B is due to wave attenuation and distortion at the coating/substrate boundary. Transverse scanning electron microscopy (SEM) of this specimen (Fig. 13) just after the first elastic wave showed a fracture in the lamellar structure parallel to the substrate. The specimen was prepared by extremely slow cutting and polishing to induce no cracking. It should be noted that a thin chromia layer, as detected by EPMA, remained at the surface of the substrate. This strongly suggests that adhesion of the glazed coating is improved by chromia. Therefore, the threshold stress (192.5 MPa) to cause initial mode II cracking is almost two times that in the as-sprayed coating (about 93.7 MPa, Fig. 8). Because the extension length of the crack is about 110  $\mu$ m, the propagation rate is estimated to be higher than 50 m/s. It was also found that the number of elastic waves in the glazed coating was extremely low compared to the as-sprayed porous coating.



**Fig. 10** Timing of elastic waves by the ADAS and conventional monitoring system for as-sprayed titania (specimen II). The top figure represents elastic waves determined by ADAS, and the bottom figure represents the acoustic emission hits from the PAC 3000 equipment.

Figure 14 shows data from specimen IV. The conventional monitoring system showed no perturbation in the AE hits. Three waves (A, B, and C) were detected by the ADAS (Fig. 15a, b, and c, respectively). Waves A and C were produced by mode II cracking and wave B by mode I cracking. Exfoliation also occurred prior to mode I cracking. Macroscopic spalling of the coating was observed at the time Wave C was recorded. Figure 16 shows the large shear delamination and the subsequent mode I fracture in the coating. The estimated rise time in the source wave was about 0.5  $\mu$ s and infers that unstable fracture, as is usually experienced in sintered ceramics, has occurred at 192.5 MPa. The elastic wave corresponding to the large mode I fracture in Fig. 15 could not be detected because of a relatively long dead time of the ADAS (about 100 ms). Specimen V suffered microshearing at 136.2 MPa and microcracking at 168.6 MPa.

On the other hand, as shown in Fig. 17, mode I cracking occurred at the low stress of 23.7 MPa for specimen VI. This specimen suffered mode II cracking at the higher stress of 69 MPa. As shown in Fig. 18, the first elastic wave corresponds to mode I cracking along the localized vertical lamellar structure in the

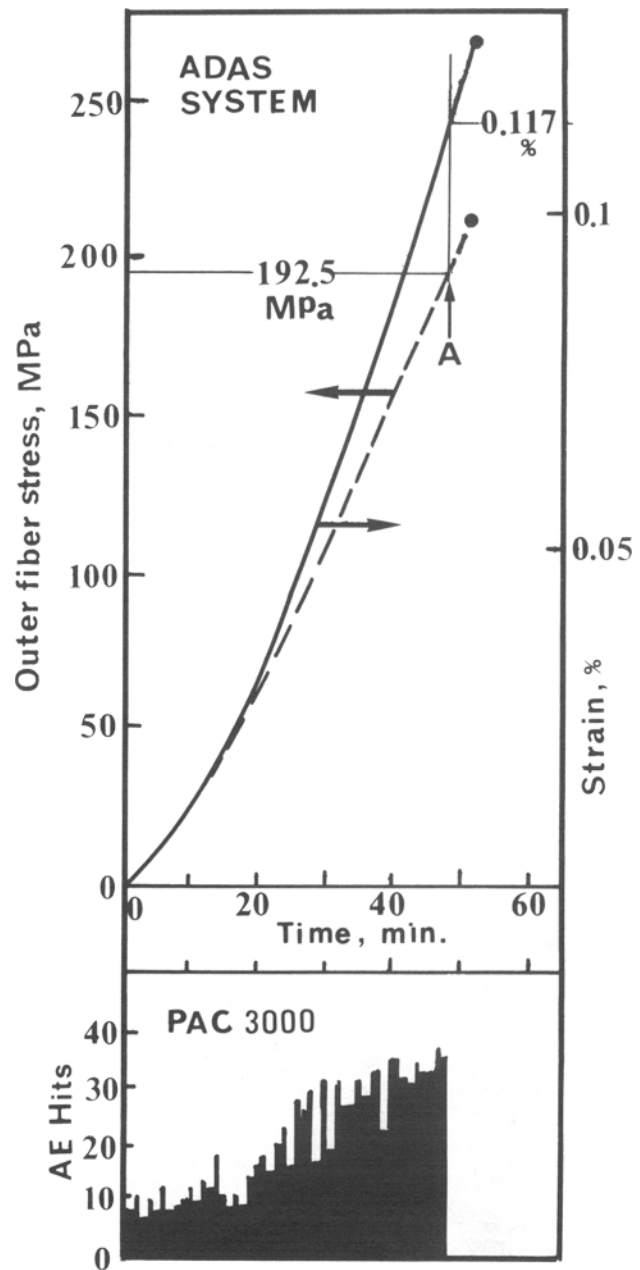


**Fig. 11** Timing of elastic waves of laser-glazed titania (specimen III).

coating. The fracture strength and mode were affected by the lamellar structure to a great extent. The coating with a lamellar structure parallel to the substrate surface (specimen III) suffered mode II cracking first, whereas the coating with a vertical lamellar structure (VI) suffered mode I cracking at an extremely low stress level.

## 6. Conclusion

An advanced AE monitoring system was used to monitor fracture strength and to elucidate the fracture modes in sprayed

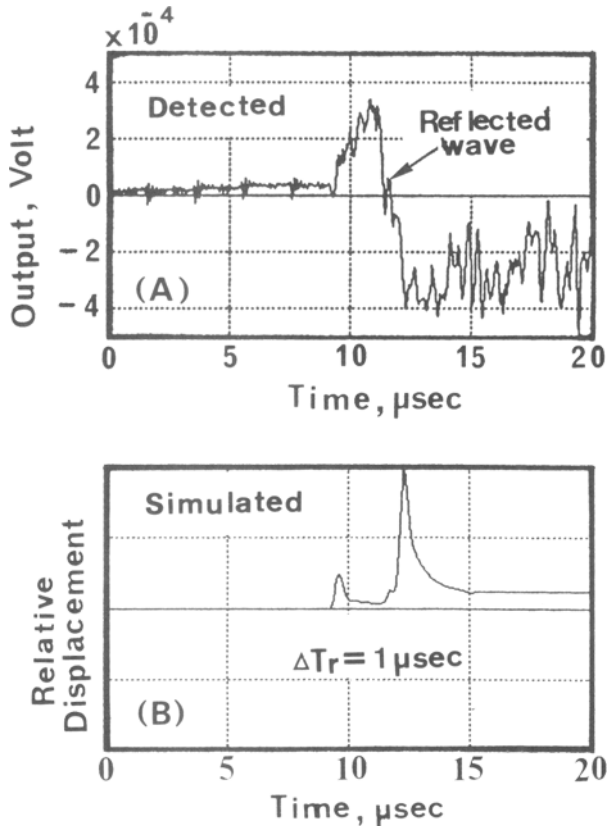


Fig. 12 Elastic wave detected at 192.5 MPa in Fig. 11 and simulated displacement to mode III exfoliation.

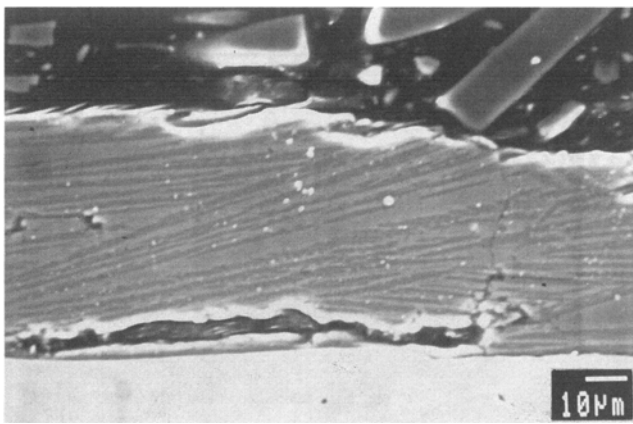


Fig. 13 Transverse SEM of bent specimen III in Fig. 11.

and laser-glazed titania coatings during four-point bending. The results are summarized as follows.

The fracture mode could be estimated by simulating the displacement at the sensor position when a displacement-sensitive monitoring system was used. On the other hand, conventional AE monitoring systems experience difficulties in elucidating mechanisms of fracture dynamics. Laser glazing of sprayed titania is possible when both thin titania and a chromium-bearing substrate were simultaneously fused under limited irradiation

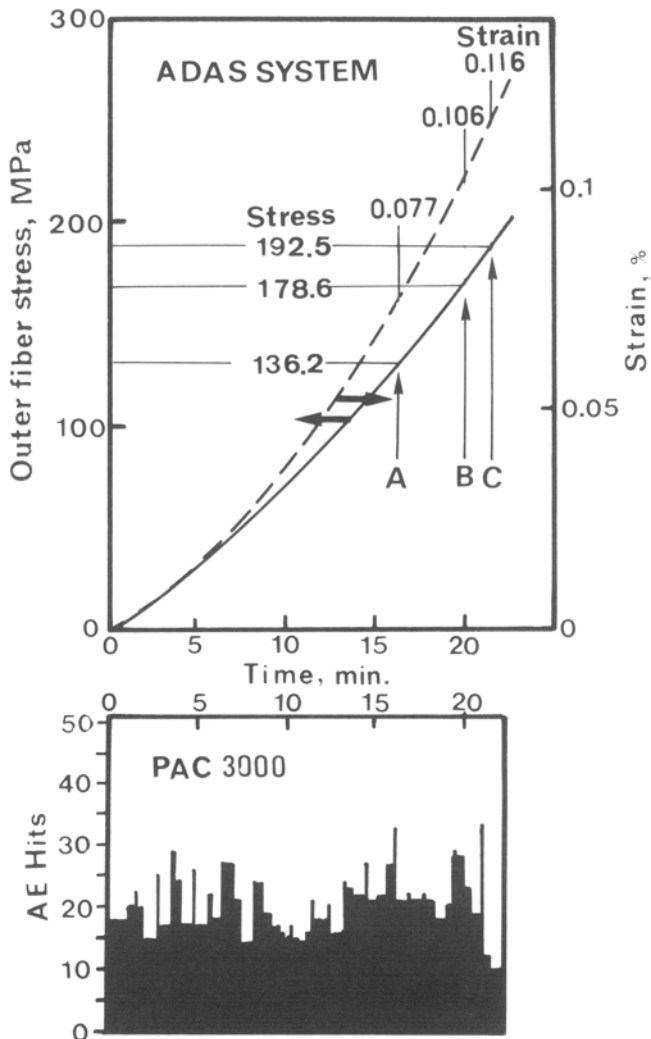


Fig. 14 Timing of elastic waves in laser-glazed titania (specimen IV).

conditions. Laser-glazed coatings possess a lamellar structure of titania and chromia.

Mode II cracking along the coating/substrate interface usually occurs prior to mode I cracking for both as-sprayed and laser-glazed coatings. The fracture strength of laser-glazed titania was higher than that of as-sprayed titania, except for one glazed coating in which mode I cracking occurred along the vertical lamellar structure.

## Acknowledgment

This work was partially supported by a grant from the Research Institute of Aoyama Gakuin University.

## References

1. M. Takemoto, Laser Surface Modification of Plasma Sprayed Oxide Ceramic Coat for Anticorrosion Performance, *High Power Laser*, Niku-Lari, Ed., Pergamon Press, 1989, p 75-88

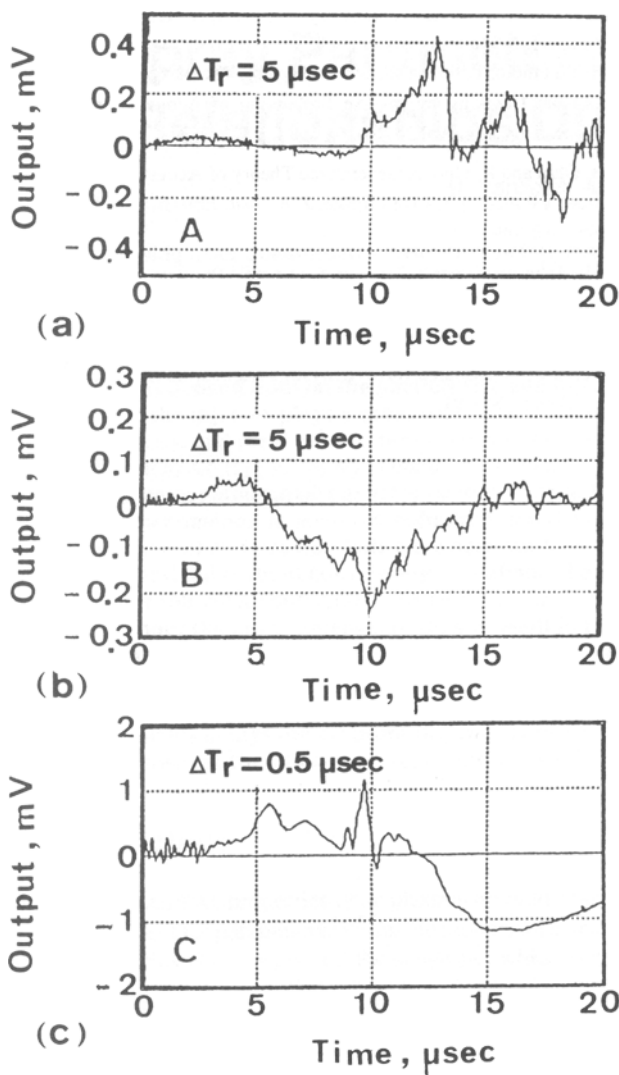


Fig. 15 Three elastic waves detected in Fig. 14.

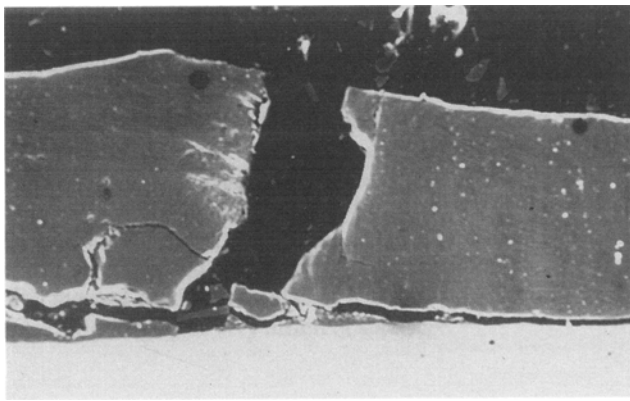


Fig. 16 Transverse SEM of specimen stressed to 192.5 MPa (Fig. 14).

2. A. Adamski and R. McPherson, Laser Processing of Thermally Sprayed Coating, *Advances in Thermal Spraying*, Welding Institute of Canada, Pergamon Press, 1986, p 555-562

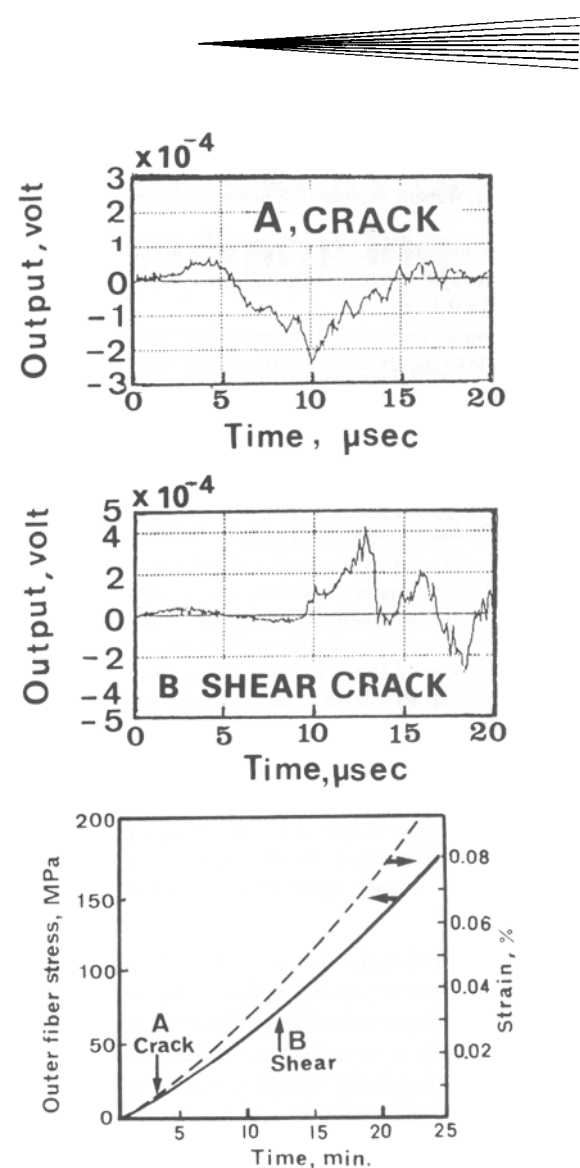


Fig. 17 Timing of two waves of laser-glazed titania (specimen VI).

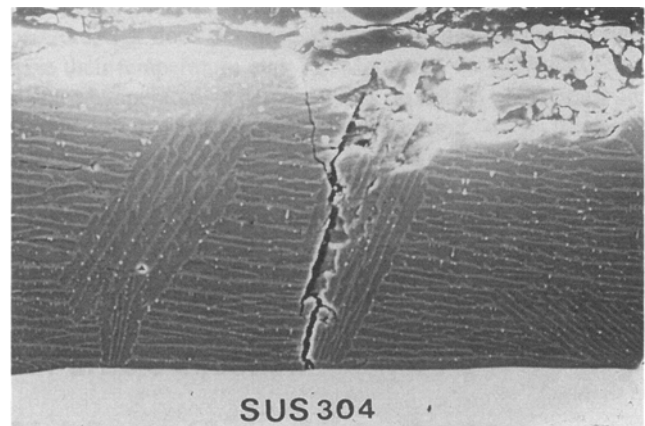


Fig. 18 Transverse SEM of bent specimen in Fig. 17.

3. N. Itamoto, N. Umenoki, and S. Endo, Laser Treatment of Plasma Ceramic Coatings, *Advances in Thermal Spraying*, Welding Institute of Canada, Pergamon Press, 1986, p 563-567

4. M. Havrd, K. Volenik, J. Wagner, and P. Mraz, Laser Treatment of Plasma Sprayed Zirconia Silicate Coatings, *Advances in Thermal Spraying*, Welding Institute of Canada, Pergamon Press, 1986, p 569-575
5. K. Mohammed Jasmin, D.R.F. West, and W.M. Steen, Laser Sealing of Plasma Sprayed Calcia-Stabilized Zirconia, *J. Mater. Sci. Lett.*, Vol 7, 1988, p 1307-1309
6. I. Zaplatynsky, Performance of Laser-Glazed Zirconia Thermal Barrier Coating in Cyclic Oxidation and Burner Rig Test, *Thin Solid Film*, Vol 95, 1982, p 275-284
7. M. Takemoto and Y. Enami, "Laser Surface Glazing of Oxide Ceramics," *Proc. Surface Engineering International Conference*, Thermal Spraying Society, Tokyo, 1988, p 103-112
8. Y. Hayashi, M. Tobari, and M. Takemoto, Fracture Strength of Laser Fusion Produced Coatings by an Elastic Wave Characterization, *Non-Destructive Characterization of Material*, T. Kishi, Ed., Tokyo, 1992, p 935-948
9. M. Takemoto, T. Terasawa, and Y. Hayashi, Microkinetics of Hydrogen Assisted Cracking by Inverse Processing of Acoustic Emission, *J. Chem. Eng. Jpn.*, Vol 24 (No. 6), 1991, p 778-783
10. M. Ohtu and K. Ono, A Generalized Theory of Acoustic Emission and Green's Function in a Half Space, *J. Acoust. Emission*, Vol 3 (No. 1), 1984, p 27-40
11. L.R. Johnson, Green's Function for Lamb's Problem, *Geophys. J. R. Astro. Soc.*, Vol 37, 1974, p 99-131
12. M. Takemoto and Y. Hayashi, Direct Measurement of Water Hammer Pressure by AE Source Wave Analyses, *J. Acoust. Emission*, Vol 7 (No. 4), 1989, p 185-191